Impacts of anisotropy coefficient and porosity on the thermal conductivity and P-wave velocity of calcarenites used as building materials of historical monuments in Morocco

Abdelaali Rahmouni, Abderrahim Boulanouar, Younes El Rhaffari, Mohammed Hraita, Aziz Zaroual, Yves Géraud, Jamal Sebbani, Abdellah Rezzouk, Bassem Nabawy

Journal of Rock Mechanics and Geotechnical Engineering 15 (2023) 1687–1699

Contents lists available at ScienceDirect

Journal of Rock Mechanics and Geotechnical Engineering

journal homepage: www.jrmge.cn

Full Length Article

Impacts of anisotropy coefficient and porosity on the thermal conductivity and P-wave velocity of calcarenites used as building materials of historical monuments in Morocco

Abdelaali Rahmouni [a,*], Abderrahim Boulanouar [b], Younes El Rhaffari [c], Mohammed Hraita [d], Aziz Zaroual [e], Yves Géraud [f], Jamal Sebbani [g], Abdellah Rezzouk [a], Bassem S. Nabawy [h]

[a] Laboratory of Solid State Physics, Department of Physics, Faculty of Science Dhar El Mahraz, Sidi Mohamed Ben Abdellah University, Fez, Morocco
[b] Laboratory of Applied Sciences, National School of Applied Sciences, Abdelmalek Essaadi University, Al Hoceima, Morocco
[c] Laboratory of Civil Engineering and Environment, Higher School of Technology of Salé, Mohammed V University, Rabat, Morocco
[d] Department of Physics, Higher Normal School, Mohammed V University, Rabat, Morocco
[e] Laboratory of Materials, Nanotechnologies and Environment, Faculty of Science, Mohammed V University, Rabat, Morocco
[f] University of Lorraine, ENSG, UMR 7359-GeoRessources, Nancy, France
[g] Mechanics and Materials Team, Faculty of Science, Mohammed V University, Rabat, Morocco
[h] Geophysical Sciences Department, National Research Centre, Cairo, Egypt

ARTICLE INFO

Article history:
Received 5 July 2022
Received in revised form
23 November 2022
Accepted 6 February 2023
Available online 13 March 2023

Keywords:
Moroccan historical monuments
Calcarenite
Thermal conductivity
P-wave velocity
Porosity
Anisotropy coefficient
Water saturation

ABSTRACT

It is essential to study the porosity, thermal conductivity, and P-wave velocity of calcarenites, as well as the anisotropy coefficients of the thermal conductivity and P-wave velocity, for civil engineering, and conservation and restoration of historical monuments. This study focuses on measuring the thermal conductivity using the thermal conductivity scanning (TCS) technique and measuring the P-wave velocity using portable equipment. This was applied for some dry and saturated calcarenite samples in the horizontal and vertical directions (parallel and perpendicular to the bedding plane, respectively). The calcarenites were selected from some historical monuments in Morocco. These physical properties were measured in the laboratory to find a reliable relationship between all of these properties. As a result of the statistical analysis of the obtained data, excellent linear relationships were observed between the porosity and both the thermal conductivity and porosity. These relationships are characterized by relatively high coefficients of determination for the horizontal and vertical samples. Based on the thermal conductivity and P-wave velocity values in these two directions, the anisotropy coefficients of these two properties were calculated. The internal structure and the pore fabric of the calcarenite samples were delineated using scanning electron microscopy (SEM), while their chemical and mineral compositions were studied using the energy dispersive X-ray analysis (EDXA) and X-ray diffraction (XRD) techniques.

1. Introduction

The capital of the Moroccan Kingdom, Rabat, has been considered a world heritage site by the United Nations Educational, Scientific and Cultural Organization (UNESCO) in 2012 (United Nations Educational, 2012). It contains architectural historical monuments of the successive rulers since the Romans (Fig. 1). It has many important architectural heritages that include numerous monuments, such as the enclosure gates of the Kasbah Oudayas, Bab Laalou, and Bab El Hadd, the minaret of Hassan mosque which rises 55 m and is considered one of the few remnants of this unfinished building, and the necropolis of Chellah situated near the downtown (Fig. 2). Thereby, the historical monuments of Rabat city in Morocco are considered among the most important archaeological Roman and Islamic sites (United Nations Educational, 2012). These monuments are characterized by the use of calcarenite stones which are widespread in the urban territory and the Rabat-Salé region.

* Corresponding author.
E-mail address: a.rahmouni@yahoo.fr (A. Rahmouni).
Peer review under responsibility of Institute of Rock and Soil Mechanics, Chinese Academy of Sciences.

https://doi.org/10.1016/j.jrmge.2023.02.008

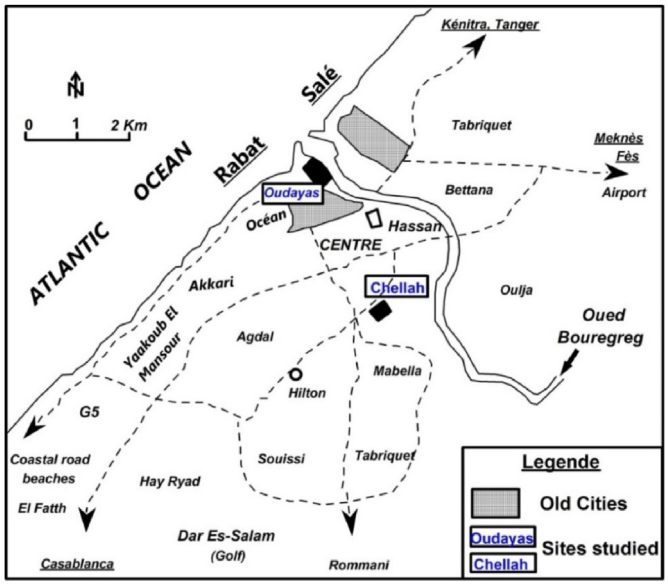

Fig. 1. Location map of the historical monuments in Rabat city, Morocco (modified after Nattah et al., 2015).

In Morocco, conservation of the heritage and historical monuments has always paid much attention to. Nonetheless, the issue of degradation of these important landmarks persists. Several kinds of research are being conducted in this context to raise awareness of the need for multidisciplinary interventions and develop non-destructive analytical methods and tests suitable for studies of architectural heritage materials (Bellitir et al., 1998; Zaouia et al., 2005; Asebriy et al., 2009; Samaouali et al., 2010; Hraita et al., 2014; Benharbit, 2017; Rahmouni et al., 2017; El Rhaffari et al., 2018; Benavente et al., 2022).

Several authors have examined the behavior of calcarenites of these monuments. The textural properties of calcarenites are primarily controlled by the weathering process. The geotechnical properties and chemical composition of calcarenites, and the presence of soluble salts in the porous system of the calcarenites were studied in detail by Zaouia et al. (2005). A multidisciplinary analysis involving geology, geophysics, and environmental properties of the historical monuments of Rabat was performed by Asebriy et al. (2009) to propose an innovative restoration and conservation technique for these monuments. In addition, Samaouali et al. (2010) investigated the degradation processes of calcarenite taken from the Chellah monument. They examined this rock to evaluate the structure of the porous network, the fluid content, and the type, distribution and amounts of the clays that were created during the deterioration of some calcarenites collected from the Chellah monument. The influence of sediment bedding, porosity, and salinity concentration on salt precipitation, as well as the evolution of calcarenite permeability and thermal conductivity over saturating and drying cycles was studied by Hraita et al. (2014). According to El Rhaffari et al. (2014), calcarenites are characterized by significant thermal and physical heterogeneity, and their thermal conductivity is closely related to the porosity.

Tests can be applied, in situ and in the laboratory, to identify the materials' physical and thermal properties. In the case of historical sites, the architectural heritage preservation recommends that building stone examinations should be conducted with the least amount of intrusion and respect for physical integrity and that a non-destructive approach for evaluating the physical and thermal properties of these building stones should be adopted. Optical scanning and ultrasonic pulse velocity are two simple low cost methods that can be applied for estimating the physical parameters of the construction stones.

Thermal conductivity, diffusivity, and effusivity, as well as the volumetric heat capacity, and the coefficient of linear thermal expansion are crucial for designing soil structures such as geothermal foundations and heat exchange systems. Consequently, thermal conductivity is required for the study of applied geophysics and geothermic issues such as determining the heat flow and deep thermal regime, and reconstructing the thermal history of sedimentary rocks. It is also required in various engineering and construction projects, including tunnels, mineral exploration, oil and gas extraction, as well as geothermal energy utilization.

Ultrasonic methods have been employed in geotechnical and civil engineering for many years. They are used in geophysical field and laboratory studies to determine the physical and thermal parameters, elastic constants, and rock weathering grades (Ozkahraman et al., 2004; Yasar and Erdogan, 2004; Kahraman and Yeken, 2008; Boulanouar et al., 2013; Rahmouni et al., 2013; 2017; Madhubabu et al., 2016; Chawre, 2018).

Different factors such as mineralogical composition, grain size and shape, presence of fluids filling the pores, density, porosity,

(a) (b)

Fig. 2. Historical monuments of Rabat: (a) The Kasbah Oudayas; and (b) The necropolis of Chellah.

pore and grain anisotropies, permeability, pressure, temperature, weathering and alteration zones, bedding planes, and fractures influence the thermal conductivity and P-wave velocity in all rocks (Birch and Clark, 1940; Birch, 1960; Horai, 1971; Gregory, 1976; Gaviglio, 1989; Clauser and Huenges, 1995; Gegenhuber and Schoen, 2012; Esteban et al., 2015; Wang et al., 2018; El Sayed et al., 2019; El Sawy et al., 2020; Zhang et al., 2021).

The interrelationship between rock physical properties, thermal conductivity, and P-wave velocity was investigated by several researchers (Huenges et al., 1997; Ozkahraman et al., 2004; Sharma and Singh, 2008; El Sayed, 2011; Pimienta et al., 2014; Ding and AuthorAnonymous, 2016; Mielke et al., 2017; Salah et al., 2020; Preux and Malinouskaya, 2021). Hartmann et al. (2005) employed the linear regression analysis to predict thermal conductivities of rocks using bulk density and P-wave velocity. Also, Kahraman (2007) applied the regression analysis to examine the P-wave velocity of dry and saturated rocks. They introduced some equations that could be applied to predict the P-wave velocity of the saturated rocks from that of the dry rocks. Boulanouar et al. (2012, 2013) explored the relationship between porosity, thermal conductivity, and P-wave velocity of the constructing rocks. Measuring the physical properties, such as porosity and density, are essential for assigning the quality of building stones. Thus, there are strong relationships between the P-wave velocity and the physical properties of the calcarenite (Rahmouni et al., 2013), which would be beneficial for people who are working in stone manufacturing plants. Selçuk and Nar (2016) studied the relationships between the P-wave velocity and the rebound number using simple and multiple regression analyses. Mielke et al. (2017) published data on the measurement of thermal conductivity and acoustic wave velocity of sedimentary, carbonate, plutonic and volcanic rock samples, and indicated that the thermal conductivity of dry porous rocks such as volcanoes and sandstones can be predicted from their acoustic wave velocity. Using simple regression approaches, strong interrelationships between the P-wave velocities and the characteristics of quartz-mica schist rocks were assigned (Chawre, 2018).

It is stated that the thermal conductivity and P-wave velocity are primarily isotropic in numerous rocks, especially volcanic and plutonic rocks (Clauser and Huenges, 1995; Ezzdine, 2009; Clauser, 2011). In contrast, many sedimentary and metamorphic rocks are mostly very anisotropic. Hence, information about anisotropy is often needed. In this context, many researchers have studied the anisotropy of rocks (Popov et al., 1999; Surma and Géraud, 2003; Vasanelli et al., 2013; Nabawy and Géraud, 2016; Shen et al., 2020; Wang et al., 2021). Gaviglio (1989) reported that the wave velocity also depends on how porous the material is and whether or not the particles are arranged in an anisotropic way. Ezzdine (2009) showed that the P-wave velocity of limestone could be measured along two main axes of anisotropy: parallel and perpendicular to the stratification direction. Kim et al. (2012) measured the anisotropic elastic moduli, P-wave velocity, and the thermal conductivity of three types of rocks. They declared that the anisotropy coefficient is significant, consequently, it should be taken into account to avoid inaccurate engineering geology applications. Macaulay et al. (2014) suggested that the difference in thermal conductivity between the saturated siltstone and sandstone was due to the presence of heterogeneity in the mineral compositions, anisotropy and densities. When estimating the thermal conductivity of the saturated sandstone and siltstone, the mineralogy, density, and bedding orientation should all be considered. Wang et al. (2018) studied causes of the thermal conductivity and P-wave velocity anisotropy coefficient variations in oil shale and indicated that the relationship between the thermal conductivity and P-wave velocity tends to take anisotropy into account.

Therefore, the present work tends to investigate the relation between the porosity, P-wave velocity, and thermal conductivity measurements for dry and saturated calcarenite samples, which were prepared considering two main axes of anisotropy, i.e. horizontal and vertical directions (parallel and perpendicular to the stratification, respectively). The anisotropy coefficients of the thermal conductivity and P-wave velocity are determined by measuring the thermal conductivity and P-wave velocity in these two directions.

2. Materials and characterization techniques

The porosity, P-wave velocity, and thermal conductivity of 10 cubic-shaped calcarenite samples of 7 cm side length were measured at the ambient conditions (room temperature and pressure) in the horizontal and vertical directions.

2.1. Sampling and samples description

The monumental buildings in Rabat are mainly built of calcarenite, a porous sedimentary rock which belongs to the Pliocene-quaternary coastal calcarenite located between Casablanca and Larache (Azouaoui et al., 2000). Calcarenite is a terminology referring to the calcium carbonate with well-developed euhedral (idiomorphic) or well-rounded anhedral (xenomorphic) crystals of the sand size, sometimes with a few quartz sand and clay minerals of mud and clay sizes (Abd El-Aal et al., 2021; Safa et al., 2021; Kassem et al., 2022). It is composed of calcium ($CaCO_3$) with a small percentage of silica (SiO_2) in the form of quartz grains (Azouaoui et al., 2000; Samaouali et al., 2017; El Rhaffari et al., 2018). The porosity of this rock was reported to be high and varied between 18% and 36% (Rahmouni et al., 2013; Hraita et al., 2016).

2.2. Porosity

The water saturation method is used to determine the porosity of the studied samples. The porous space that is available for water under vacuum conditions is the definition of total porosity. According to AFPC-AFREM (1997), it is measured using the concept of triple-weighing procedure.

The representative rock samples were weighed to obtain their dry (W_{dry}), fully saturated (W_{sat}) and hydrostatical (W_{hyd}) masses using a digital balance (ControLab D0627.058) of precision 0.001 g. The samples were saturated under vacuum with degassed deionized water. The $W_{sat} - W_{dry}$ difference gives the weight of water that has entered the porous network. The $W_{sat} - W_{hyd}$ difference gives the weight of the water occupying the same volume as the sample. This gives

$$W_{sat} - W_{dry} = \rho_w V_{pore} \tag{1}$$

$$W_{sat} - W_{hyd} = \rho_w V_{bulk} \tag{2}$$

where ρ_w is the density of water at the temperature of the experiment, V_{pore} is the pore volume, and V_{bulk} is the bulk volume of the studied sample.

The porosity φ of a given sample corresponds to the volume of pores divided by the bulk volume of the measured sample. It can be expressed as

$$\varphi = \frac{V_{pore}}{V_{bulk}} = \frac{W_{sat} - W_{dry}}{W_{sat} - W_{hyd}} \tag{3}$$

2.3. Thermal conductivity scanning method

Several experimental methods have been proposed for measuring the thermal properties of materials (Beck, 1957; Popov et al., 1999; Hartmann et al., 2005; Smith et al., 2013; Macaulay et al., 2014; Nabawy and Géraud, 2016; Korte et al., 2017). The split bar method is used on cylindrical samples with a diameter between 30 mm and 50 mm. This technique necessitates the use of known thermal conductivity standards. The measurement time can be as short as 10–15 min, the measurement error is just 2% (Blackwell and Spafford, 1987), but the surface condition of the sample must be irreproachable to achieve the best thermal contact (Beck, 1957; Pribnow and Sass, 1995; Popov et al., 1999). The guarded hot plate method is used for measuring the thermal characteristics of construction materials. It operates by forcing a 10 °C temperature difference between three parallel plates in a symmetric design, with the cold plate in the center (typically at 15 °C) and the two hot plates above and below the samples (usually at 25 °C). Two samples of the same material are placed in between. The test stops when the thermal equilibrium is achieved and the subsequently measured values of thermal conductivity are stable. At a given temperature, several measurements needed to obtain the validated values last about 6–7 h (Santa et al., 2017). Abdulagatov et al. (2015) measured the thermal conductivity and thermal diffusivity of natural sandstone samples using the laser-flash method. In this method, the thermal system is a sample of flat surfaces that receives on its front face a heat flux supplied by a laser, and records the evolution of the temperature on its rear face, either by contact with thermocouples or without contact with an infrared detector. It is distinguished by a short measuring duration, less than other traditional contact methods. Another technique, i.e. heating needle, is based on the idea that there is a point source of heat in an infinite medium (Rosener, 2007), and is in the form of a probe included in a needle. This method permits the measurement of thermal conductivity based on the sample's temperature and saturation with an uncertainty of less than 12%.

For techniques that necessitate direct contact between the measuring probe and the sample, the contact resistances are hardly determined because they depend on both the proper contact and the applied physical conditions. Limiting the contact resistances, therefore, amounts to limiting errors in the measurement (Popov et al., 1999). In this study, we are interested in the thermal conductivity scanning (TCS) method for measuring the thermal conductivity.

Popov et al. (1985) created the fundamentals of the TCS method and apparatus, which is considered the standard for thermal conductivity measurements on rock materials. The experimental equipment of TCS is a mobile block with two temperature sensors and a laser heat source positioned parallel to the axis of movement. It allows for the measurement of the sample's temperature before and after heating (Fig. 3). For a measurement line, the sensors and laser heat source move at a constant speed ($V = 4.99$ mm/s) close at hand the surface of the sample, which makes it possible to obtain a thermal conductivity profile.

The two temperature sensors (T1 and T2) are used to measure how much the energy input changes the temperature. After heating, the difference in temperature between the hot and cold sensors is used for estimating the thermal properties of the sample. The relationship between the temperature at x, $\theta(x)$, and the thermal conductivity (Popov et al., 1999) is given as follows:

$$\theta(x) = \frac{q}{2\pi x\lambda} \tag{4}$$

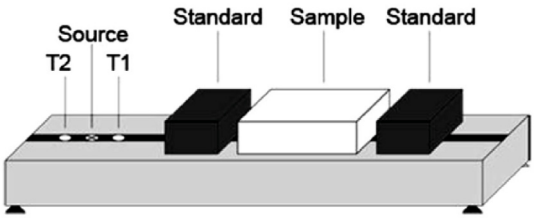

Fig. 3. TCS measurement principle.

where q is the source power, x is the distance between the heat source and the sensor, and λ is the thermal conductivity.

The thermal conductivity of the studied sample is obtained by aligning this sample using a standard with the thermal conductivity of $\lambda_{std} = 1.35$ W/(m K):

$$\lambda(x) = \lambda_{std}\frac{\theta_{std}}{\theta(x)} \tag{5}$$

The range of measured conductivity values is between 0.2 W/(m K) and 70 W/(m K), and the measurement error is less than 3% (Popov et al., 1999).

The sample preparation procedure in this study is quite simple. A layer of black paint is applied to the surface of the sample to avoid a variation in heat absorption due to color variations on the surface of the sample. To perform a measurement, it suffices to position the sample as well as the two standards on the apparatus (Fig. 3). Measurements can be performed on multiple samples at once using a computer-controlled system.

2.4. P-wave velocity measurements

P-wave velocity is primarily dependent on the elastic properties which are influenced by some variables, including mineral composition, density, porosity, stress, pore pressure, fluid type, saturation, and pore shape (Nur and Simmons, 1969; Nur, 1971; Han et al., 1986; Kassab and Weller, 2015; Yu et al., 2016; Salah et al., 2020).

The P-wave velocity (V_P) was calculated by measuring the ultrasonic wave velocity through the sample. For this objective, a digital ultrasonic testing instrument Proceq TICO was used. At room temperature and normal pressure, the P-wave velocity (V_P) was measured for each sample. It was determined by the tester that processed the arrival time of the wave between the transmitter and the receiver. It has a set of cylindrical piezoelectric transducers with a frequency of 54 kHz. A shear gel was used to improve the connection, which conformed to the recommendations of the International Society for Rock Mechanics (1978) for the P-wave velocity measurements of rocks.

2.5. Anisotropy coefficient

Even if a material is composed of strongly anisotropic minerals, it is usually either isotropic or anisotropic. If there is anisotropy, it means that the values of the directional physical properties of rock, such as thermal conductivity and P-wave velocity, change depending on how the samples are oriented (parallel to the bedding plane in the horizontal direction while the other is perpendicular to the bedding plane in the vertical direction). The measured thermal values in the directions parallel ($\lambda_{//}$) and perpendicular ($\lambda_{\perp}$) to the bedding plane are used to determine the thermal anisotropy coefficient (Jorand et al., 2013):

$$A_\lambda = \frac{\lambda_{//}}{\lambda_\perp} \quad (6)$$

where A_λ is the anisotropy coefficient of the thermal conductivity.

For the P-wave measurements, the following expression was used to estimate the anisotropy coefficient of P-wave velocity (Kassab and Weller, 2019):

$$A_{V_P} = \frac{V_{P//}}{V_{P\perp}} \quad (7)$$

where A_{V_P} is the anisotropy coefficient of the P-wave velocity; and $V_{P//}$ and $V_{P\perp}$ are the P-wave velocities in the directions parallel and perpendicular to the bedding plane, respectively.

The determined physical properties and the anisotropy coefficients of thermal conductivity and P-wave velocity for dry and saturated samples are presented in Tables 1 and 2.

2.6. Scanning electron microscopy and energy dispersive X-ray analysis techniques

For delineating the microstructures and the chemical composition of the studied samples, some additional samples were selected representatively, imaged using the scanning electron microscope (SEM), and analyzed using the energy dispersive X-ray analysis (EDXA) technique. Samples were prepared firstly by coating them with a thin layer of carbon to improve the images' quality. Therefore, caution should be considered during interpreting the C and O_2 contents. Imaging was applied at a high vacuum with 10 kV voltage and magnification power of 500–2000. The scanning microscopy is supported by the EDXA tool so that imaging and the chemical analysis were performed contemporaneously in such a way that EDXA was applied for a shot spot selected from the image area. Two EDXA spots were considered for each sample, i.e. the vertical and horizontal directions (Table 3). Delineating the internal structures of porous samples and checking their chemical composition using EDXA were successfully applied by many authors (Safa et al., 2021). To support the EDXA results and interpretation, the scanned and EDXA analyzed samples were also investigated using the X-ray diffraction analysis (XRD) technique to define and reveal the mineral composition of the bulk samples using EMPYREAN diffractometer system at 4.02–11.2 keV. The data were identified according to the PANalytical XRD software. The samples were ground carefully to an adequate size and then analyzed in the range of 2θ up to 90°. Results of the XRD data interpretation are presented in Table 4.

Table 1
The thermal conductivity, anisotropy coefficient, and porosity of the calcarenite samples.

Sample	$\lambda_{d\perp}$ (W/(m K))	$\lambda_{d//}$ (W/(m K))	$\lambda_{s\perp}$ (W/(m K))	$\lambda_{s//}$ (W/(m K))	$A_{\lambda d}$	$A_{\lambda s}$	ϕ (%)
1	1.227	1.185	1.905	1.989	0.97	1.04	19.62
2	1.198	1.149	1.822	1.94	0.96	1.06	22.31
3	1.102	1.052	1.794	1.851	0.95	1.03	25.69
4	1.068	0.971	1.761	1.803	0.91	1.02	27.86
5	1.005	0.899	1.731	1.71	0.89	0.99	29.82
6	0.884	0.802	1.69	1.746	0.91	1.03	31.07
7	0.876	0.768	1.681	1.667	0.88	0.99	33.5
8	0.946	0.866	1.716	1.75	0.92	1.02	34.6
9	0.912	0.852	1.675	1.688	0.93	1.01	35.07
10	0.87	0.79	1.673	1.69	0.91	1.01	35.83
Mean	1.009	0.933	1.745	1.783	0.92	1.02	29.54
Min	0.87	0.768	1.673	1.667	0.88	0.99	19.62
Max	1.227	1.185	1.905	1.989	0.97	1.06	35.83
SD	0.133	0.15	0.076	0.111	0.03	0.02	5.59

Note: SD is the standard deviation; Min and Max mean the minimum and maximum values, respectively; and subscripts 'd' and 's' denote the dry and saturated samples, respectively.

Table 2
The P-wave velocity and anisotropy coefficient of the studied samples.

Sample	$V_{Pd\perp}$ (km/s)	$V_{Pd//}$ (km/s)	$V_{Ps\perp}$ (km/s)	$V_{Ps//}$ (km/s)	$A_{V_{Pd}}$	$A_{V_{Ps}}$
1	4.37	4.18	4.5	4.26	0.96	0.95
2	4.2	4	4.39	4.2	0.95	0.96
3	3.8	3.56	4.1	3.87	0.94	0.94
4	3.94	3.55	4.04	3.75	0.9	0.93
5	3.83	3.42	3.88	3.46	0.89	0.89
6	3.52	3.1	3.69	3.34	0.88	0.91
7	3.64	3.15	3.55	3.21	0.87	0.9
8	3.45	3.12	3.78	3.43	0.9	0.91
9	3.61	3.27	3.65	3.3	0.91	0.9
10	3.49	3.09	3.72	3.37	0.89	0.91
Mean	3.79	3.44	3.93	3.62	0.91	0.92
Min	3.45	3.09	3.55	3.21	0.87	0.89
Max	4.37	4.18	4.5	4.26	0.96	0.96
SD	0.3	0.38	0.32	0.37	0.03	0.02

3. Results and discussion

In this study, the physical properties measured for dry and saturated calcarenite samples are the porosity (ϕ), thermal conductivities in the horizontal and vertical directions ($\lambda_{//}$ and $\lambda_\perp$) and P-wave velocities in the horizontal and vertical directions ($V_{P//}$ and $V_{P\perp}$).

Generally, porosity affects the physical properties such as density, thermal conductivity, seismic velocity, permeability, pore size, and pore size distribution. The mean porosity obtained by averaging all porosity data is 29.54%. Table 1 displays porosity values ranging from 19.62% to 35.83% for all the studied samples, indicating that the sample compositions are heterogeneous.

Thermal conductivity values were determined for all the studied dry and saturated samples in both the horizontal and vertical directions. The horizontal conductivity ($\lambda_{//}$) in the dry and saturated states ranges from 0.768 W/(m K) to 1.185 W/(m K) and from 1.667 W/(m K) to 1.989 W/(m K), with the average of 0.933 W/(m K) and 1.783 W/(m K), respectively. The vertical conductivity values range from 0.87 W/(m K) to 1.227 W/(m K) and from 1.673 W/(m K) to 1.905 W/(m K) in dry and saturated states, with the average of 1.009 W/(m K) and 1.745 W/(m K), respectively. The thermal conductivity values of the saturated samples are much higher than that of dry samples (Table 1). The anisotropy coefficient of thermal conductivity is obtained from Eq. (6) for all samples. This anisotropy coefficient refers to the ratio of conductivities in two main directions, i.e. parallel and perpendicular to the bedding plane. The anisotropy coefficient varies between 0.88 and 0.97 for dry samples and between 0.99 and 1.06 for saturated samples.

The vertical velocity ($V_{P\perp}$) of most calcarenite samples studied is slightly greater than the horizontal velocity ($V_{P//}$). In the dry and saturated states, the vertical P-wave velocity ranges from 3.45 km/s to 4.37 km/s and from 3.55 km/s to 4.5 km/s, while the horizontal P-wave velocity ranges from 3.09 km/s to 4.18 km/s and from 3.21 km/s to 4.26 km/s, respectively. The average vertical velocity is 3.79 km/s and 3.93 km/s for the dry and saturated samples, and the corresponding average horizontal velocity is 3.44 km/s and 3.62 km/s, respectively (Table 2). All samples show similar P-wave anisotropy coefficient in both dry and saturated states, with values ranging from 0.87 to 0.96.

Principally, the thermal conductivity of rocks is controlled by their mineralogical composition, porosity, texture, and pore fluids.

Table 3
The chemical analysis (in mass %) and mineral composition of the studied samples using the EDXA technique. Analysis was applied to some spots in the same imaged sample to reveal the overall composition.

Sample	C	O	Mg	Al	Si	Ca
S-2 ⊥	41.55 ± 0.12	29.45 ± 0.23	0.52 ± 0.44	2.08 ± 0.06	5.9 ± 0.1	20.49 ± 0.28
S-2//	39.82 ± 0.11	29.59 ± 0.27	–	0.54 ± 0.04	1.03 ± 0.05	29.02 ± 0.35
S-2 Av.	40.69 ± 0.12	29.52 ± 0.25	0.26 ± 0.22	1.31 ± 0.05	3.47 ± 0.08	24.76 ± 0.32
S-4 ⊥	23.87 ± 0.09	37.66 ± 0.28	–	0.52 ± 0.04	2.32 ± 0.07	35.64 ± 0.37
S-4//	24.4 ± 0.12	35.52 ± 0.32	0.39 ± 0.04	1.3 ± 0.06	5.81 ± 0.12	32.59 ± 0.43
S-4 Av.	24.14 ± 0.11	36.29 ± 0.3	0.2 ± 0.02	0.91 ± 0.05	4.07 ± 0.09	34.11 ± 0.4
S-7 ⊥	28.71 ± 0.12	49.48 ± 0.36	-	1.1 ± 0.06	1.61 ± 0.08	19.1 ± 0.35
S-7//	32.43 ± 0.24	49.1 ± 0.67	-	-	1.92 ± 0.16	16.55 ± 0.61
S-7 Av.	30.57 ± 0.18	49.24 ± 0.52	–	0.55 ± 0.03	1.77 ± 0.12	17.83 ± 0.48
S-10 ⊥	24.17 ± 0.14	38.97 ± 0.45	-	-	2.11 ± 0.11	34.75 ± 0.59
S-10//	38.76 ± 0.22	35.53 ± 0.52	-	-	1.66 ± 0.12	20.36 ± 0.57
S-10 Av.	31.47 ± 0.18	37.25 ± 0.49	–	–	1.89 ± 0.12	27.56 ± 0.58

Note: ⊥ and//refer to the measurements in the direction perpendicular and parallel to the bedding plane, respectively; and Av. Denotes the average value.

Table 4
The mineral composition of the studied samples based on the XRD interpretation.

Sample	Mineral composition (%)	
	Calcite	Quartz
2	94.02	5.98
4	94.61	5.39
7	94.54	5.46
10	97.97	2.03

In both the horizontal and vertical directions, the thermal conductivity of the studied samples is displayed as a function of porosity in Fig. 4.

The relationship between the porosity and the thermal conductivity indicates that the thermal conductivity decreases as the porosity increases. In the literature, some correlations have been presented to determine the porosity of rocks employing thermal conductivity data (Popov et al., 2003; El Sayed, 2011; Boulanouar et al., 2012; Korte et al., 2017; Zerrouki et al., 2019). In the direction parallel to the bedding plane, Popov et al. (2003) discovered a relationship between the thermal conductivity and porosity of limestone and sandstone with regression coefficients of 0.97 and 0.9, respectively. According to Ozkahraman et al. (2004), the thermal conductivity versus porosity of sedimentary rocks has a correlation coefficient of 0.97. Boulanouar et al. (2012) found a linear relationship between dry and saturated rock properties, with correlation coefficients of 0.91 and 0.68, respectively. For sedimentary rocks, Zerrouki et al. (2019) estimated the correlation coefficients between the thermal conductivity and porosity, 0.44 for cemented samples and 0.73 for uncemented samples.

In this study, the relationship between the thermal conductivity and porosity can be represented by the following equations:

$$\lambda_{d//} = 1.680 - 0.025\phi \left(R^2 = 0.88\right) \quad (8)$$

$$\lambda_{d\perp} = 1.682 - 0.022\phi \left(R^2 = 0.9\right) \quad (9)$$

$$\lambda_{s//} = 2.336 - 0.018\phi \left(R^2 = 0.89\right) \quad (10)$$

$$\lambda_{s\perp} = 2.130 - 0.013\phi \left(R^2 = 0.91\right) \quad (11)$$

where R^2 is the coefficient of determination.

The P-wave velocity depends on various characteristics, including mineral composition, porosity, presence of cracks and fractures, and fluid content. In both the horizontal and vertical directions, the results of P-wave velocity measurements versus porosity are shown in Fig. 5. Several correlation equations have been developed to evaluate the porosity of rocks based on P-wave velocity measurements (Martin and Brown, 1996; Koesoemadinata and McMechan, 2004; Boulanouar et al., 2013; Kassab and Weller, 2015; Yu et al., 2016; Chawre, 2018; Salah et al., 2020; Miah, 2021). Good coefficients of determination have been identified (R^2 = 0.9, 0.86, 0.89, and 0.88 for dry and saturated samples, respectively), indicating that a reliable estimation of the porosity of the studied samples may be derived from P-wave velocity data using the proposed equations:

$$V_{Pd//} = 5.377 - 0.065\phi \left(R^2 = 0.9\right) \quad (12)$$

$$V_{Pd\perp} = 5.314 - 0.051\phi \left(R^2 = 0.86\right) \quad (13)$$

$$V_{Ps//} = 5.516 - 0.064\phi \left(R^2 = 0.89\right) \quad (14)$$

$$V_{Ps\perp} = 5.535 - 0.054\phi \left(R^2 = 0.88\right) \quad (15)$$

Many researchers have previously correlated the P-wave velocity and thermal conductivity using regression analysis (Ozkahraman et al., 2004; El Sayed, 2011; Kim et al., 2012; Boulanouar et al., 2013; Esteban et al., 2015; Wang et al., 2018; El Sayed and El Sayed, 2019). In this study, good relationships between the P-wave velocity and thermal conductivity in the horizontal and vertical directions are observed, as shown in Fig. 6. It is found that the increase in the thermal conductivity increases the P-wave velocity. The following equations can be used to describe the fitting lines:

$$V_{Pd//} = 1.123 + 2.486\lambda_{d//} \left(R^2 = 0.92\right) \quad (16)$$

$$V_{Pd\perp} = 1.611 + 2.154\lambda_{d\perp} \left(R^2 = 0.86\right) \quad (17)$$

$$V_{Ps//} = -2.54 + 3.461\lambda_{s//} \left(R^2 = 0.89\right) \quad (18)$$

$$V_{Ps\perp} = -3.191 + 4.081\lambda_{s\perp} \left(R^2 = 0.93\right) \quad (19)$$

The correlations between the directional parameters, i.e. the thermal conductivity and P-wave velocity in both the vertical and

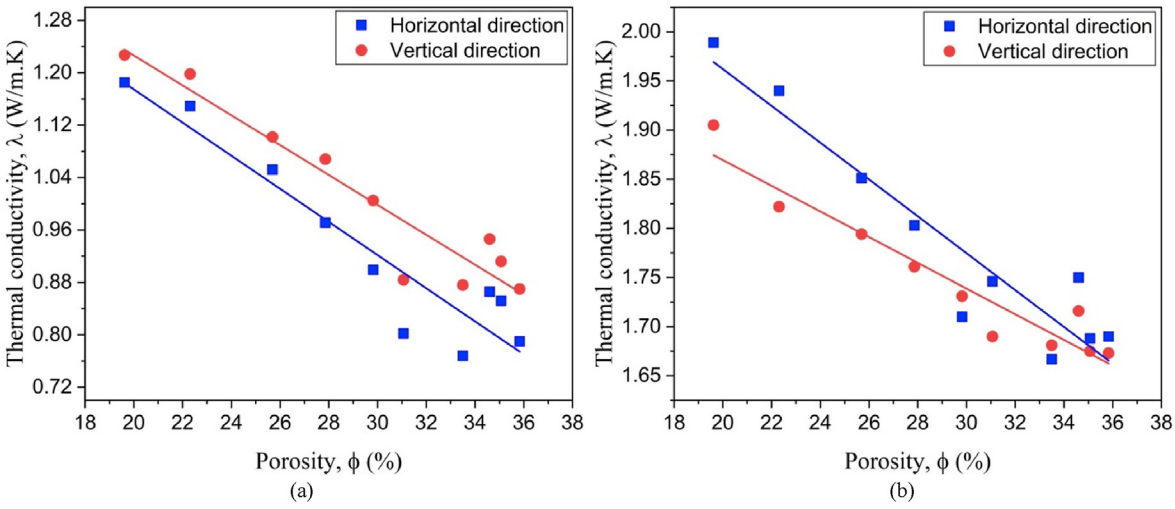

Fig. 4. Horizontal and vertical thermal conductivities ($\lambda_{//}$ and $\lambda_{\perp}$) as functions of the porosity (ϕ) for (a) dry and (b) saturated samples.

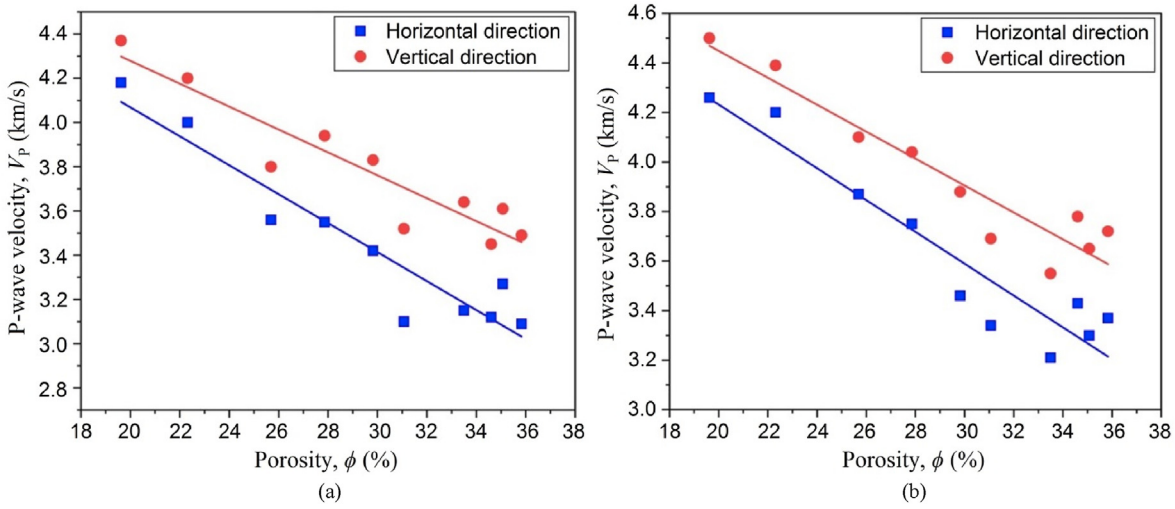

Fig. 5. Horizontal and vertical P-wave velocities ($V_{P//}$ and $V_{P\perp}$) as functions of the porosity (φ) for (a) dry and (b) saturated samples.

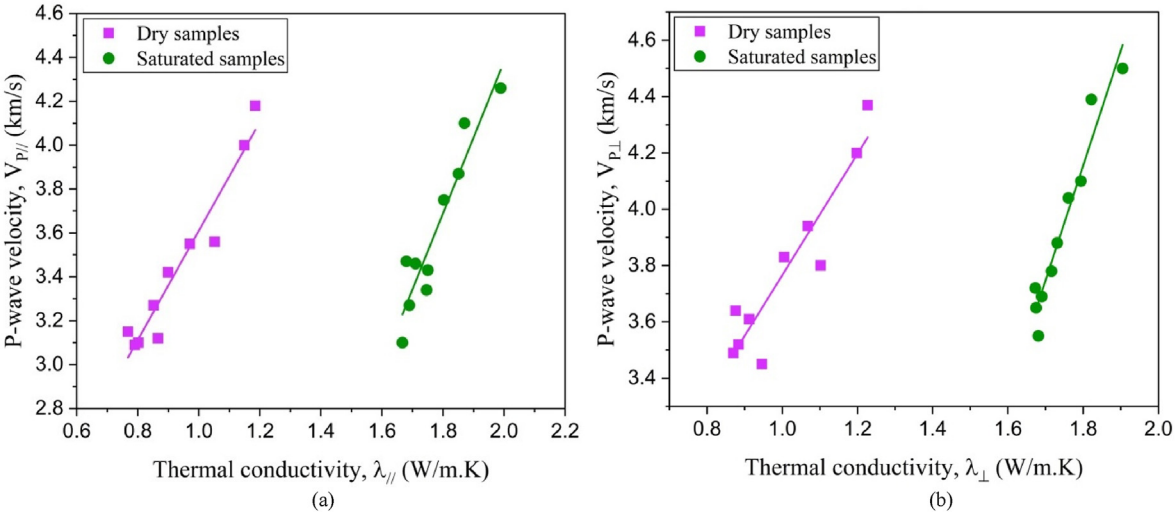

Fig. 6. (a) Horizontal P-wave velocity ($V_{P//}$) versus horizontal thermal conductivity ($\lambda_{//}$) and (b) vertical P-wave velocity ($V_{P\perp}$) versus vertical thermal conductivity ($\lambda_{\perp}$) for dry and saturated samples.

horizontal directions for dry and saturated samples are illustrated in Fig. 7. The cross plot between the horizontal thermal conductivity ($\lambda_{//}$) and the vertical thermal conductivity ($\lambda_{\perp}$) shows that the vertical thermal conductivity is greater than the horizontal thermal conductivity in the dry state (Fig. 7a). In saturated state, the horizontal thermal conductivity is greater than the vertical thermal conductivity for the majority of samples. Implication of water saturation on the thermal conductivity anisotropy coefficient is shown in Fig. 7a. Saturating the calcarenite samples with degassed water caused the thermal anisotropy coefficient values to shift much closer to the unity (isotropic line) than that of the dry samples, i.e. saturating the studied samples with water reduced their thermal anisotropy coefficient. Dry samples are more thermally anisotropic than the saturated samples. Several experimental studies (Clauser and Huenges, 1995; Popov et al., 2003; Gruescu et al., 2007) revealed that the pore form and water saturation degree affect the thermal conductivity. Clauser and Huenges (1995) and Gruescu et al. (2007) found that for clays, the closer the pore shape is to spherical, the less the conductivity is influenced by saturation, and the more flattened the pore shape is, the greater the effect of water saturation is. The results of the measurements described in the work of Popov et al. (2003) showed that for saturated porous rocks, thermal conductivity values are larger compared to dry rocks. Wang et al. (2018) measured the thermal conductivity of dry oil shale in the directions perpendicular and parallel to the bedding planes. The results showed that the conductivity values are higher in the parallel direction.

The cross plot of the horizontal P-wave velocity ($V_{P//}$) versus the vertical P-wave velocity ($V_{P\perp}$) (Fig. 7b) reveals that the vertical P-wave velocity is greater than the horizontal P-wave velocity for all dry and saturated samples. Many researchers have investigated the vertical and horizontal variations of P-wave velocity (Martin and Brown, 1996; Koesoemadinata and McMechan, 2004; Kahraman, 2007; Ezzdine, 2009; Wang et al., 2018; Kassab and Weller, 2019; Zerrouki et al., 2022). Kahraman (2007) conducted ultrasonic tests perpendicular to the bedding plane for sedimentary rocks. The obtained results showed that the P-wave velocity in saturated samples was greater than that in dry samples. Wang et al. (2018) determined the P-wave velocity of dry oil shale in the vertical and horizontal bedding directions, and the results indicated that higher values of the P-wave velocity were obtained in the horizontal direction. Kassab and Weller (2019) presented experimental results measuring the P-wave velocity of dry carbonate rocks. They found that the vertical velocity was slightly greater than the horizontal velocity.

Fig. 8a shows that there is a very good direct proportional relationship between the thermal conductivities of dry and saturated samples in the horizontal and vertical directions, with coefficients of determination of $R^2 = 0.92$ and 0.93, respectively. This means that the thermal conductivity of saturated samples can be predicted from the thermal conductivity of dry samples according to the following equations:

$$\lambda_{s//} = 1.119 + 0.711\lambda_{d//} \left(R^2 = 0.92\right) \tag{20}$$

$$\lambda_{s\perp} = 1.188 + 0.551\lambda_{d\perp} \left(R^2 = 0.93\right) \tag{21}$$

The relationship between the P-wave velocities of dry and saturated samples, as indicated in Fig. 8b, shows a good proportional relation with coefficients of determination of $R^2 = 0.91$ and 0.84 in the horizontal and vertical directions, respectively.

From the P-wave velocity of dry samples, it is possible to predict the P-wave velocity of saturated samples. These relationships are shown below:

$$V_{Ps//} = 0.377 + 0.941V_{Pd//} \left(R^2 = 0.91\right) \tag{22}$$

$$V_{Ps\perp} = 0.321 + 0.953V_{Pd\perp} \left(R^2 = 0.84\right) \tag{23}$$

Fig. 9 illustrates the relationship between the anisotropies of P-wave velocity and thermal conductivity for dry and saturated samples. As a result of P-wave velocity and thermal conductivity studies, it is possible to identify and differentiate between the structural and cracking anisotropies. Results show that the anisotropy of thermal conductivity is directly related to the anisotropy coefficient of the P-wave velocity, with coefficients of determination of $R^2 = 0.91$ and 0.8 for dry and saturated samples, respectively. These findings are useful because they can be used to estimate the anisotropy of a given property. The anisotropy coefficients of the P-wave velocity and thermal conductivity are therefore correlated to each other, and can be estimated as follows:

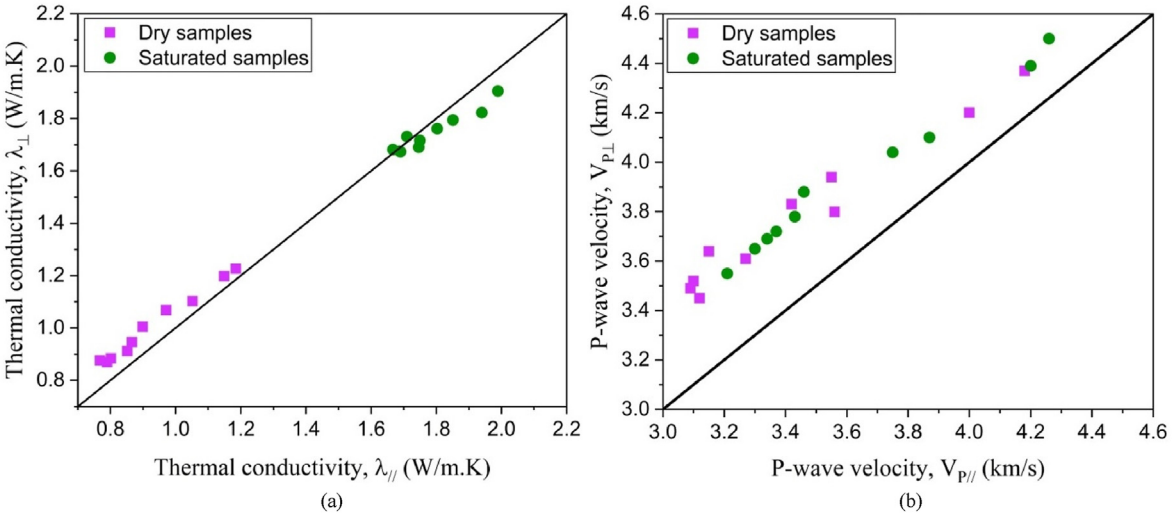

Fig. 7. The cross plots (a) between the horizontal thermal conductivity ($\lambda_{//}$) and the vertical thermal conductivity ($\lambda_{\perp}$) and (b) between the horizontal P-wave velocity ($V_{P//}$) and the vertical P-wave velocity ($V_{P\perp}$) for dry and saturated samples.

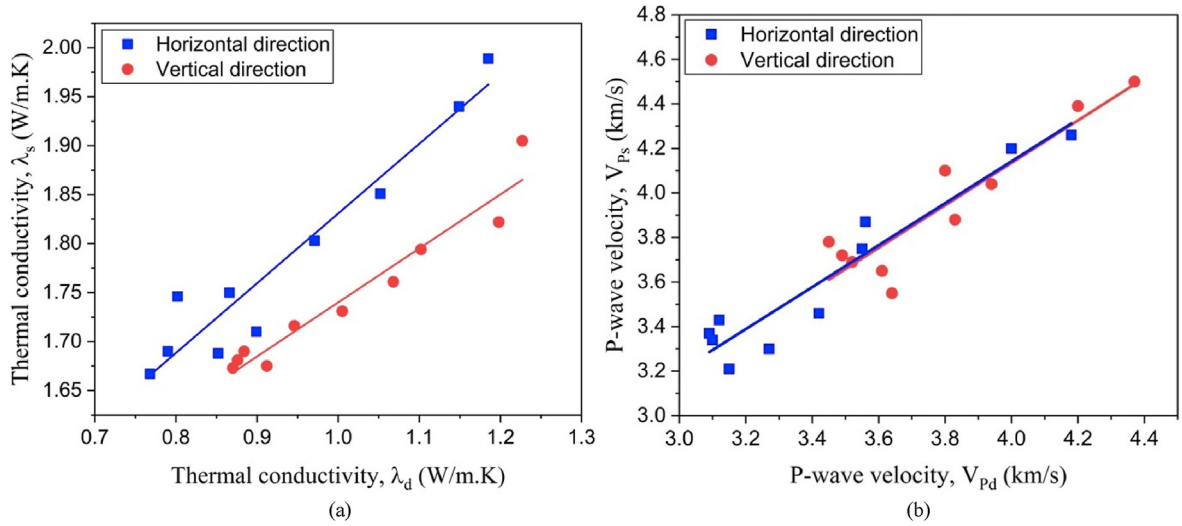

Fig. 8. Relationship between (a) thermal conductivities and (b) P-wave velocities of dry and saturated samples in the horizontal and vertical directions.

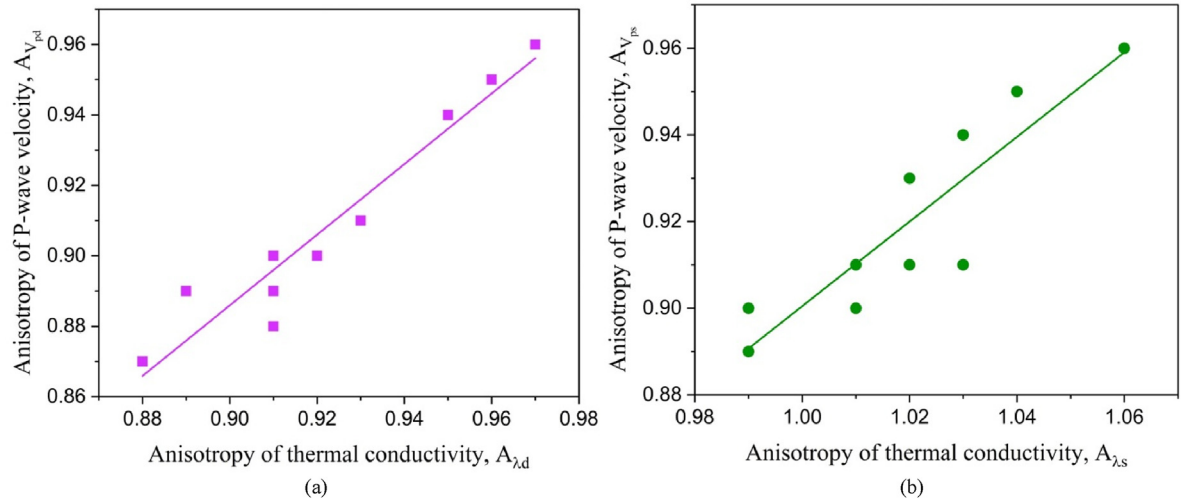

Fig. 9. Relationship between the anisotropy coefficients of the P-wave velocity and thermal conductivity for (a) dry and (b) saturated samples.

$$A_{V_{Pd}} = -0.0163 + 1.0025A_{\lambda d} \left(R^2 = 0.91\right) \quad (24)$$

$$A_{V_{Ps}} = -0.0757 + 0.9761A_{\lambda s} \left(R^2 = 0.8\right) \quad (25)$$

SEM is a successful technique for revealing the microstructures of the studied samples. Imaging sample S-2 indicates a highly porous structure with intergranular porosity and many intersecting pore channels and vugs (Fig. 10a). Crystals are primarily in the pseudo sparite sizes (17.5–28 μm, Fig. 10a). Micrite to micro-sparite sizes (calcilutite, 1.9–5.18 μm, Fig. 10b) are also encountered indicating a secondary phase of diagenetic cementation by Ca-bearing solutions. Dissolution and leaching out the cement of this sample may be indicated by the presence of some microfossil relics (500 μm length) and fossil molds increasing the secondary porosity value (Fig. 10c). For sample S-4, crystallization seems to be more well-developed than sample S-2 with dominated pseudo sparite crystal sizes (12.96–34.94 μm, Fig. 10d) and intercrystalline porosity slightly reduced by the developed tinny micrite (calcilutite) filling the pore spaces (1.14–2.11 μm, Fig. 10e). Also, traces of dolomicrite (dololutite) crystals and clay minerals (mostly kaolinite booklets) are present as attachments to the crystals' surface and as a pore-filling material. The crystal size of sample S-7 is much coarser than the other samples, where the crystals are described as well-developed sparite to micro-sparite crystals (36.28–82.92 μm, Fig. 10f), which seem to adhere to each other with relatively low intercrystalline porosity (negligible to poor porosity (<10%), Fig. 10f). For sample S-10, the crystal size decreases to the pseudo sparite sizes. Surfaces of the sparite crystals are covered by many tiny micrite crystals and micro-sparite crystals (calcilutite) as a diagenetic cementation phase (Fig. 10g). Pore spaces are filled by many tinny crystals and clay minerals as a pore-filling material, i.e. porosity has been improved (15%–20%, Fig. 10h).

Thereby, the SEM studies indicate different pore types (intergranular, pore molds, vugs, and microfractures), which are scattered randomly. Also, it is worth mentioning that the thermal and sonic anisotropies of the saturated samples depend on the spatial distribution of the crystals and the pore spaces, while in the dry state, anisotropies are dependent only on the spatial distribution of solid constituents (crystals). This means that the final anisotropy coefficient values of the saturated calcarenite samples are primarily

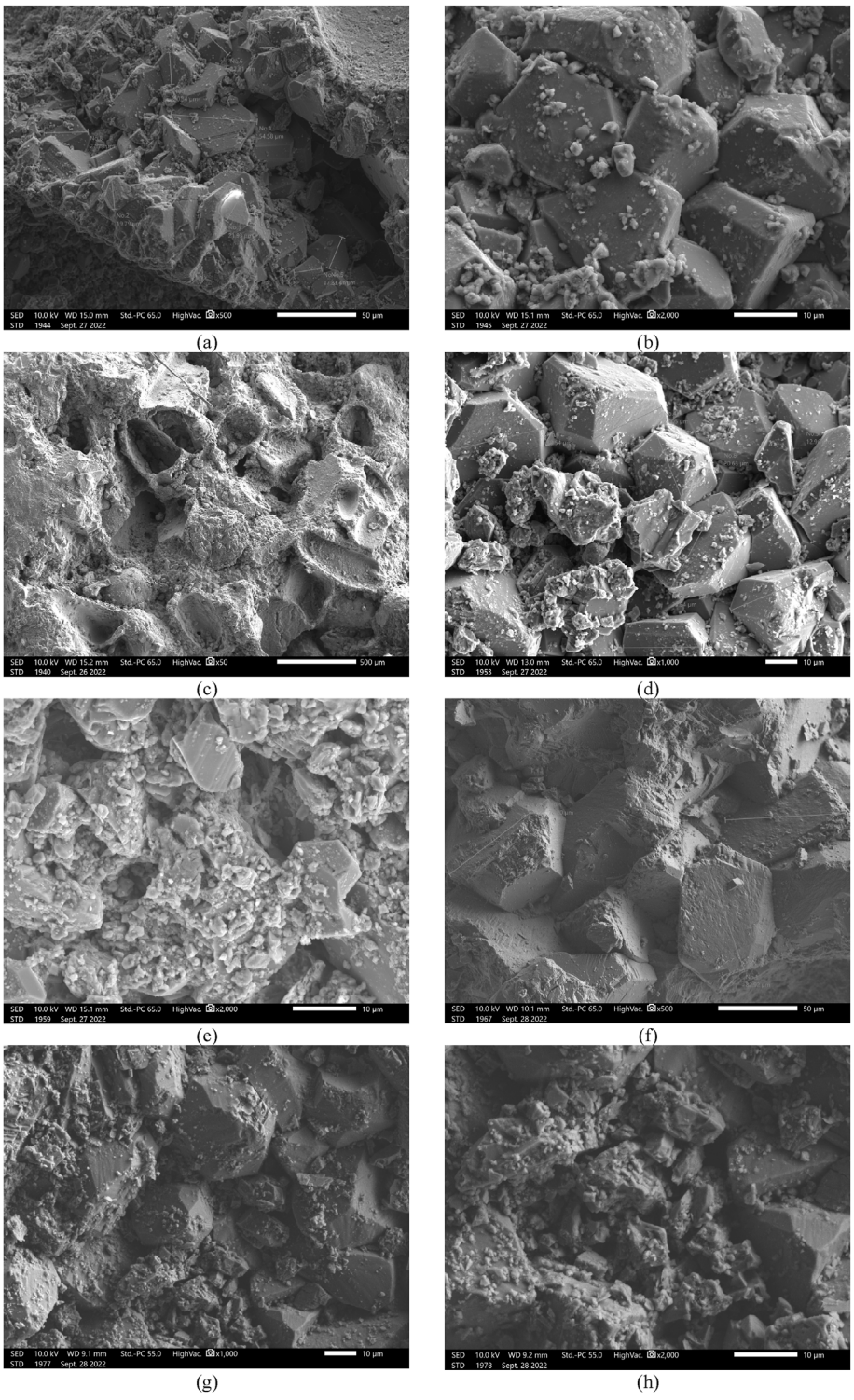

Fig. 10. Revealing the microstructures of the studied samples using SEM techniques: (a–c) Sample S-2; (d, e) Sample S-4; (f) Sample S-7; and (g, h) Sample S-10.

attributed by two anisotropic components, namely the crystal network and the spatial distribution of the pore space network which is complicated and highly connected due to the high porosity values of the studied calcarenite (19.62%–35.83% with the average of 29.54%, Table 1).

Eventually, the EDXA of the studied samples indicates the dominance of calcite composition ($CaCO_3$) in all samples with a small sand and clay content (Table 3 and Fig. 11). The absence of potash feldspars and plagioclase or the presence of some relics of their altered crystals (Table 3 and Fig. 10) may be the reason for the presence of a few traces of Al-silicate clay content. However, the highest sand content is assigned for samples S-2 and S-4 (Fig. 11a and b) with traces of dolomite or Mg-rich calcite in these two samples (Table 3). Concerning the EDXA results of S-7 and S-10, it is stated that these two samples are chemically and mineralogically homogeneous in composition. Therefore, the mineral composition impact and the spatial distribution of grains/crystals on the anisotropy coefficient of dry samples are somewhat limited.

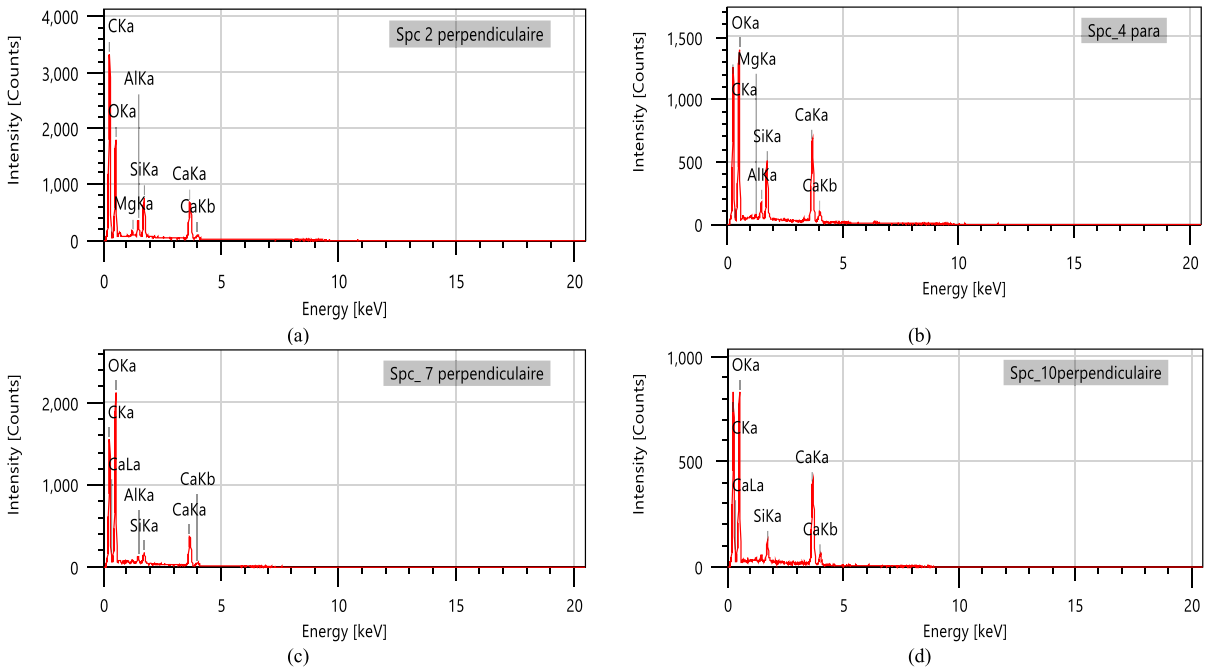

Fig. 11. The chemical composition of the analyzed samples using the EDXA technique applied for samples (a) S-2, (b) S-4, (c) S-7, and (d) S-10.

Similarly, the XRD data interpretation of the bulk samples indicates that the studied samples are mineralogically homogeneous with a dominance of the calcite composition (~94.5%, Table 4). However, the sample 10 indicates a slight increase in the calcite content (~98%, Table 4) which is considered ineffective to control the physical behavior of this sample. The counts versus 2θ plot indicates sharper counting peak of the calcite at 2θ of ~29° for sample 10 than that for sample 2, and less sharpening peak for the main quartz peak at 2θ of ~26.6° (Fig. 12). However, the slight difference in the physical behavior of this sample should be attributed to a slight increase in the effective porosity (35.85%, Table 1) than the other samples due to the dissolution and leaching out process as a predominate diagenetic factor.

4. Conclusions

(1) The internal crystal structure and the pore network spatial distribution were imaged using SEM, which indicated that most samples are composed of calcarenite (sparite) crystals with some calcilutites (micrite) with low contents of quartz grains and clay minerals. The pore network is highly connected but also highly complicated in three-dimensional (3D) cases, which is composed of intergranular, intercrystalline, microfractures, and vuggy pore spaces.

(2) The thermal conductivity and P-wave velocity measurements are performed on dry and saturated samples in the horizontal and vertical directions relative to the bedding plane.

(3) The TCS technique allows the estimation of the thermal conductivities of the studied samples. The results indicate that the thermal conductivity of calcarenites decreases with increasing porosity and that the water saturation has an impact on the thermal conductivity. These results indicate that the thermal conductivity of the calcarenite is dependent on its porosity, pore network structure, and the interstitial fluid saturation.

(4) The P-wave velocity measurements reveal that the sonic velocities of the saturated samples are greater than those of the dry samples. Besides, the P-wave velocity of the dry and

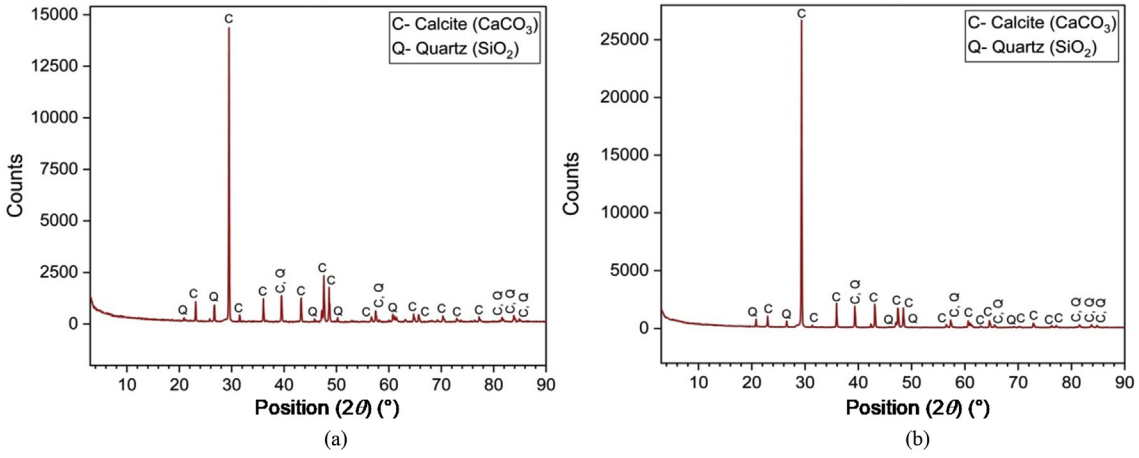

Fig. 12. The mineral composition of the analyzed samples based on the XRD data applied for samples (a) S-2 and (b) S-10.

saturated calcarenites decreases as the porosity increases. The thermal conductivity and P-wave velocity versus porosity plots for the dry and saturated samples indicate the dependence of both parameters on the porosity, where the obtained best-fit lines for these two plots are characterized by high coefficients of determination.

(5) The thermal conductivity and P-wave velocity values are higher in the saturated state than those in the dry state. However, plotting the thermal conductivity and the P-wave velocity for the dry samples against those for the saturated samples indicates that values of these two parameters in the saturated state are closely related to the corresponding values in the dry state. This is due to the fully-saturated pore network system in the velocity and thermal conductivities of the saturated samples. However, somewhat similar anisotropy coefficients are obtained for the P-wave velocity and the thermal conductivity values for all dry and saturated samples (with the ratios of average values of $A_{V_{Pd}} : A_{V_{Ps}} = 0.91: 0.92$ and $A_{\lambda d}: A_{\lambda s} = 0.92{:}1.02$, respectively). The EDXA results indicated that the studied samples are chemically homogeneous and in turn homogenous in their mineral composition. This means that the anisotropy coefficient of the calcarenite samples in the dry state is relatively low due to the homogeneity of their solid components.

(6) The XRD data interpretation supported the EDXA technique, where it revealed the homogeneity in the mineral composition of the studied samples (with the calcite content of 94.02%–97.97%).

(7) The strongest correlations were obtained between thermal conductivity and P-wave velocity anisotropies. These results can be used to estimate the anisotropy coefficient of other physical properties when the anisotropy coefficient of a related property is known.

(8) Measurements of the thermal conductivity and P-wave velocity may be used to estimate the porosity as well as the anisotropy coefficient. It is important to consider the conservation and restoration of historical monuments in this setting, which allows the existence of a quantifiable quantity on the site at a low cost and without causing any damage. This is a very interesting point because the P-wave velocity can be directly linked to the porosity and thermal conductivity.

Declaration of competing interest

The authors declare that they have no known competing financial interests or personal relationships that could have appeared to influence the work reported in this paper.

References

Abd El-Aal, A.K., Zakhera, M., Khalifa, M.A., Talha Qadri, S.M., Nabawy, B.S., 2021. Carbonate strength classification based on depositional textures and fossil content of the Lower Eocene Drunka Formation, Assiut Area, central Egypt. J. Pet. Sci. Eng. 207, 109061.

Abdulagatov, I.M., Abdulagatov, Z.Z., Kallaev, S.N., Bakmaev, A.G., Ranjith, P.G., 2015. Thermal-diffusivity and heat-capacity measurements of sandstone at high temperatures using laser flash and DSC methods. Int. J. Thermophys. 36, 658–691.

Afpc-Afrem, 1997. Détermination de la masse volumique apparente et de la porosité accessible à l'eau. Toulouse, France. In: Méthodes recommandées pour la mesure des grandeurs associées à la durabilité: Compte-rendu des journées techniques, pp. 121–124 (in French).

Asebriy, L., Cherkaoui, T.E., El Amrani, I.E., et al., 2009. Deterioration processes on archaeological sites of Chellah and Oudayas (world cultural heritage, Rabat, Morocco): restoration test and recommendations. Ital. J. Geosci. 128 (1), 157–171.

Azouaoui, H., El Hatimi, N., El Yamine, N., 2000. Les formations plio-quaternaires de la région de Casablanca (Maroc): aspects sédimentologique et géotechnique. Bull. Eng. Geol. Environ. 59, 59–74.

Beck, A.E., 1957. A steady state method for the rapid measurements of the thermal conductivity of rocks. J. Sci. Instrum. 34 (5), 186–189.

Bellitir, D., Nijs, R., Asebriy, L., Aberkan, M., 1998. Evolution de la calcarénite dans les constructions; vitesse d'altération en fonction des facteurs naturels et industriels. Mines, Geol. Energ. 57, 83–88 (in French).

Benavente, D., Martinez-Martinez, J., Galiana-Merino, J.J., Pla, C., de Jongh, M., Garcia-Martinez, N., 2022. Estimation of uniaxial compressive strength and intrinsic permeability from ultrasounds in sedimentary stones used as heritage building materials. J. Cult. Herit. 55, 346–355.

Benharbit, M., 2017. Cement mortar restorations and disorders in the archaeological site of Chellah. Int. J. Adv. Eng. Res. Sci. 4 (8), 11–14.

Birch, A.F., 1960. The velocity of compressional waves in rocks to 10 kilobars: 1. J. Geophys. Res. 65 (4), 1083–1102.

Birch, A.F., Clark, H., 1940. The thermal conductivity of rocks and its dependence upon temperature and composition. Am. J. Sci. 238 (8), 529–558.

Blackwell, D.D., Spafford, R.E., 1987. Experimental methods in continental heat flow. Methods Exp. Phys. 24, 189–226.

Boulanouar, A., Rahmouni, A., Boukalouch, M., Géraud, Y., El Amrani, E.I., Harnafi, M., Sebbani, J., 2012. Corrélation entre la vitesse d'onde P et la conductivité thermique des matériaux hétérogènes et poreux. MATEC Web of Conf 2, 05004 (in French).

Boulanouar, A., Rahmouni, A., Boukalouch, M., Samaouali, A., Géraud, Y., Harnafi, M., Sebbani, J., 2013. Determination of thermal conductivity and porosity of building stone from ultrasonic velocity measurements. Geomaterials 3 (4), 138–144.

Chawre, B., 2018. Correlations between ultrasonic pulse wave velocities and rock properties of quartz-mica schist. J. Rock Mech. Geotech. Eng. 10 (3), 594–602.

Clauser, C., 2011. Thermal storage and transport properties of rocks, I: heat capacity and latent heat. In: Gupta, H.K. (Ed.), Encyclopedia of Solid Earth Geophysics. Springer, Dordrecht, Netherlands, pp. 1423–1431.

Clauser, C., Huenges, E., 1995. Thermal conductivity of rocks and minerals. In: Ahrens, T.J. (Ed.), Rock Physics and Phase Relations: A Handbook of Physical Constants, vol. 3. The American Geophysical Union, Washington, D.C., USA, pp. 105–126.

Ding, Q.L., Song, S.B., 2016. Experimental investigation of the relationship between the P-wave velocity and the mechanical properties of damaged sandstone. Adv. Mater. Sci. Eng. 2016, 7654234.

El Rhaffari, Y., Hraita, M., Rahmouni, A., Samaouali, A., Boukalouch, M., Geraud, Y., 2018. Elemental chemical analysis by X-ray fluorescence of calcarenite stones used in historical monuments building of Rabat (Morocco). MATEC Web of Conf 149, 02057.

El Rhaffari, Y., Hraita, M., Samaouali, A., Boukalouch, M., Géraud, Y., 2014. Thermal and petrophysical characteristics of calcarenite rocks used in the construction of monuments of Rabat. Rev. Rom. Mater. 44 (2), 153–159.

El Sawy, M.Z., Abuhagaza, A.A., Nabawy, B.S., Lashin, A., 2020. Rock typing and hydraulic flow units as a successful tool for reservoir characterization of Bentiu-Abu Gabra sequence, Muglad basin, southwest Sudan. J. Afr. Earth Sci. 171, 103961.

El Sayed, A.A., 2011. Thermophysical study of sandstone reservoir rocks. J. Pet. Sci. Eng. 76, 138–147.

El Sayed, A.A., El Sayed, N.A., 2019. Thermal conductivity calculation from P-wave velocity and porosity assessment for sandstone reservoir rocks. Geothermics 82, 91–96.

El Sayed, A.M., Abu Seda, H.H., El Sayed, N.A., 2019. Effect of fluid saturation on acoustic wave velocity for sandstone reservoirs. IOP Conf. Ser. Earth Environ. Sci. 221, 012046.

Esteban, L., Pimienta, L., Sarout, J., Piane, C.D., Haffen, S., Geraud, Y., Timms, N.E., 2015. Study cases of thermal conductivity prediction from P-wave velocity and porosity. Geothermics 53, 255–269.

Ezzdine, R., 2009. Endommagement des monuments historiques en maçonnerie. PhD Thesis, vol. 1. Université Bordeaux, Bordeaux, France (in French).

Gaviglio, P., 1989. Longitudinal waves propagation in a limestone: the relationship between velocity and density. Rock Mech. Rock Eng. 22 (4), 299–306.

Gruescu, C., Giraud, A., Homand, F., Kondo, D., Do, D.P., 2007. Effective thermal conductivity of partially saturated porous rocks. Int. J. Solid Struct. 44 (3–4), 811–833.

Gegenhuber, N., Schoen, J., 2012. New approaches for the relationship between compressional wave velocity and thermal conductivity. J. Appl. Geophys. 76, 50–55.

Gregory, A.R., 1976. Fluid saturation effects on dynamic elastic properties of sedimentary rocks. Geophysics 41 (5), 895–921.

Han, D.H., Nur, A., Morgan, D., 1986. Effect of porosity and clay content on wave velocities in sandstones. Geophysics 51 (11), 2093–2107.

Hartmann, A., Rath, V., Clauser, C., 2005. Thermal conductivity from core and well log data. Int. J. Rock Mech. Min. Sci. 42 (7–8), 1042–1055.

Horai, K., 1971. Thermal conductivity of rock-forming minerals. J. Geophys. Res. 76 (5), 1278–1308.

Hraita, M., El Rhaffari, Y., Fadili, G., Samaouali, A., Géraud, Y., Boukalouch, M., 2016. Role of sediment bedding orientation and salt concentration on the evolution of petrophysical properties of calcarenite stone during salt weathering cycles by sodium chloride. Rev. Rom. Mater. 46 (2), 242–249.

Hraita, M., El Rhaffari, Y., Samaouali, A., Géraud, Y., Boukalouch, M., 2014. Petrophysical, petrographical and mineralogical characterization of calcarenite rock used for monumental building in Morocco. Rev. Rom. Mater. 44 (4), 365–374.
Huenges, E., Bücker, C., Lippmann, E., Lauterjung, J., Kern, H., 1997. Seismic velocity, density, thermal conductivity and heat production of cores from the KTB pilot hole. Geophys. Res. Lett. 24 (3), 345–348.
International Society for Rock Mechanics (ISRM), 1978. Suggested method for determining sound velocity. Int. J. Rock Mech. Min. Sci. Geomech. Abstr. 15 (2), 53–58.
Jorand, R., Vogt, C., Marquart, G., Clauser, C., 2013. Effective thermal conductivity of heterogeneous rocks from laboratory experiments and numerical modeling. J. Geophys. Res. Solid Earth 118 (10), 5225–5235.
Kahraman, S., 2007. The correlations between the saturated and dry P-wave velocity of rocks. Ultrasonics 46 (4), 341–348.
Kahraman, S., Yeken, T., 2008. Determination of physical properties of carbonate rocks from P-wave velocity. Bull. Eng. Geol. Environ. 67, 277–281.
Kassab, M.A., Weller, A., 2015. Study on P-wave and S-wave velocity in dry and wet sandstones of Tushka region, Egypt. Egypt. J. Petrol. 24 (1), 1–11.
Kassab, M.A., Weller, A., 2019. Anisotropy of permeability, P-wave velocity and electrical resistivity of upper cretaceous carbonate samples from tushka area, western desert, Egypt. Egypt. J. Petrol. 28 (2), 189–196.
Kassem, A.A., Osman, O.A., Nabawy, B.S., Baghdady, A.R., Shehata, A.A., 2022. Microfacies analysis and reservoir discrimination of channelized carbonate platform systems: an example from the Turonian Wata Formation, Gulf of Suez, Egypt. J. Pet. Sci. Eng. 212, 110272.
Kim, H., Cho, J.W., Song, I., Min, K.B., 2012. Anisotropy of elastic moduli, P-wave velocities, and thermal conductivities of Asan gneiss, Boryeong shale, and Yeoncheon schist in Korea. Eng. Geol. 147–148, 68–77.
Koesoemadinata, A.P., McMechan, G.A., 2004. Effects of diagenetic processes on seismic velocity anisotropy in near-surface sandstone and carbonate rocks. J. Appl. Geophys. 56 (3), 165–176.
Korte, D., Kaukler, D., Fanetti, M., Cabrera, H., Daubront, E., Franko, M., 2017. Determination of petrophysical properties of sedimentary rocks by optical methods. Sediment. Geol. 350, 72–79.
Macaulay, D.B., Bouazza, A., Singh, R.M., Wang, B., 2014. Thermal properties of some Melbourne soils and rocks. Aust. GeoMech. 49 (2), 31–44.
Madhubabu, N., Singh, P.K., Kainthola, A., Mahanta, B., Tripathy, A., Singh, T.N., 2016. Prediction of compressive strength and elastic modulus of carbonate rocks. Measurement 88, 202–213.
Martin, N.W., Brown, R.J., 1996. Compressional velocity, seismic attenuation and permeability relationships for sandstones from WOSPP. CREWES Res. Rep. 8, 5, 1–5.19.
Miah, M.I., 2021. Improved prediction of shear wave velocity for clastic sedimentary rocks using hybrid model with core data. J. Rock Mech. Geotech. Eng. 13 (6), 1466–1477.
Mielke, P., Bär, K., Sass, I., 2017. Determining the relationship of thermal conductivity and compressional wave velocity of common rock types as a basis for reservoir characterization. J. Appl. Geophys. 140, 135–144.
Nabawy, B.S., Géraud, Y., 2016. Impacts of pore- and petro-fabrics, mineral composition and diagenetic history on the bulk thermal conductivity of sandstones. J. Afr. Earth Sci. 115, 48–62.
Nattah, I., Touhami, A.O., Benkirane, R., Douira, A., 2015. Etude des lichens du site de Chellah, monument historique de Rabat, dont Placidium squamulosum (Ach.) Breuss, nouvelle espèce pour la flore lichénique du Maroc. Int. J. Innov. Sci. Res. 19 (2), 377–401 (in French).
Nur, A., 1971. Effects of stress on velocity anisotropy in rocks with cracks. J. Geophys. Res. 76 (8), 2022–2034.
Nur, A., Simmons, G., 1969. The effect of saturation on velocity in low porosity rocks. Earth Planet Sci. Lett. 7 (2), 183–193.
Ozkahraman, H.T., Selver, R., Isik, E.C., 2004. Determination of the thermal conductivity of rock from P-wave velocity. Int. J. Rock Mech. Min. Sci. 41 (4), 703–708.
Pimienta, L., Sarout, J., Esteban, L., Piane, C.D., 2014. Prediction of rocks thermal conductivity from elastic wave velocities, mineralogy and microstructure. Geophys. J. Int. 197 (2), 860–874.
Popov, Y., Tertychnyi, Y., Romushkevich, R., Korobkov, D., Pohl, J., 2003. Interrelations between thermal conductivity and other physical properties of rocks: experimental data. Pure Appl. Geophys. 160, 1137–1161.
Popov, Y.A., Berezin, V.V., Semionov, V.G., Korosteliov, V.M., 1985. Complex detailed investigations of the thermal properties of rocks on the basis of a moving point source. Izvestiya Phys. Solid Earth 21 (1), 64–70.
Popov, Y.A., Pribnow, D.F.C., Sass, J.H., Williams, C.F., Burkhardt, H., 1999. Characterization of rock thermal conductivity by high-resolution optical scanning. Geothermics 28, 253–276.
Preux, C., Malinouskaya, I., 2021. Thermal conductivity model function of porosity: review and fitting using experimental data. Oil Gas Sci. Technol. 76, 66.
Pribnow, D.F.C., Sass, J.H., 1995. Determination of thermal conductivity for deep boreholes. J. Geophys. Res. Solid Earth 100 (B6), 9981–9994.
Rahmouni, A., Boulanouar, A., Boukalouch, M., Géraud, Y., Samaouali, A., Harnafi, M., Sebbani, J., 2013. Prediction of porosity and density of calcarenite rocks from P-wave velocity measurements. Int. J. Geosci. 4 (9), 1292–1299.
Rahmouni, A., Boulanouar, A., Samaouali, A., Boukalouch, M., Géraud, Y., Sebbani, J., 2017. Prediction of elastic and acoustic behaviors of calcarenite used for construction of historical monuments of Rabat, Morocco. J. Rock Mech. Geotech. Eng. 9 (1), 74–83.
Rosener, M., 2007. Etude pétrophysique et modélisation des effets des transferts thermiques entre roche et fluide dans le contexte géothermique de Soultz-Sous-Forets. Ph.D. Thesis. Université Luis Pasteur, Strasbourg, France (in French).
Safa, M.G., Nabawy, B.S., Basal, A.M.K., Omran, M.A., Lashin, A., 2021. Implementation of a petrographical and petrophysical workflow protocol for studying the impact of heterogeneity on the rock typing and reservoir quality of reefal limestone: a case study on the nullipore carbonates in the Gulf of Suez. Acta Geol. Sin. – Engl. Ed. 95 (5), 1746–1762.
Salah, M.K., Alqudah, M., Monzer, A.J., David, C., 2020. Petrophysical and acoustic characteristics of Jurassic and Cretaceous rocks from Central Lebanon. Carbonates Evaporites 35, 12.
Samaouali, A., El Rhaffari, Y., Hraita, M., Laanab, H., Oudrhiri Géraud, Y., 2017. Porous network structure and total porosity of rocks used in historical monument challah. Rev. Rom. Mater. 47 (2), 222–229.
Samaouali, A., Laanab, L., Boukalouch, M., Géraud, Y., 2010. Porosity and mineralogy evolution during the decay process involved in the Chellah monument stones. Environ. Earth Sci. 59, 1171–1181.
Santa, G.D., Peron, F., Galgaro, A., Cultrera, M., Bertermann, D., Mueller, J., Bernardi, A., 2017. Laboratory measurements of gravel thermal conductivity: an update methodological approach. Energy Proc. 125, 671–677.
Selçuk, L., Nar, A., 2016. Prediction of uniaxial compressive strength of intact rocks using ultrasonic pulse velocity and rebound-hammer number. Q. J. Eng. Geol. Hydrogeol. 49 (1), 67–75.
Sharma, P.K., Singh, T.N., 2008. Correlation between P-wave velocity, impact strength index, slake durability index and uniaxial compressive strength. Bull. Eng. Geol. Environ. 67, 17–22.
Shen, H., Li, X., Li, Q., Wang, H., 2020. A method to model the effect of pre-existing cracks on P-wave velocity in rocks. J. Rock Mech. Geotech. Eng. 12 (3), 493–506.
Smith, D.S., Alzina, A., Bourret, J., et al., 2013. Thermal conductivity of porous materials. J. Mater. Res. 28 (17), 2260–2272.
Surma, F., Géraud, Y., 2003. Porosity and thermal conductivity of the Soultz-sous-Forêts granite. Pure Appl. Geophys. 160, 1125–1136.
United Nations Educational, 2012. Scientific and Cultural Organization. UNESCO). World heritage list. https://whc.unesco.org/en/list/1401/.
Vasanelli, E., Sileo, M., Calia, A., Aiello, M.A., 2013. Non-destructive techniques to assess mechanical and physical properties of soft calcarenitic stones. Procedia Chem. 8, 35–44.
Wang, G., Yang, D., Kang, Z., Zhao, J., 2018. Anisotropy in thermal recovery of oil shale – Part 1: thermal conductivity, wave velocity and crack propagation. Energies 11 (1), 77.
Wang, Y., Wang, Z., Shi, L., et al., 2021. Anisotropic differences in the thermal conductivity of rocks: a summary from core measurement data in east China. Minerals 11 (10), 1135.
Yasar, E., Erdogan, Y., 2004. Correlating sound velocity with the density, compressive strength and Young's modulus of carbonate rocks. Int. J. Rock Mech. Min. Sci. 41 (5), 871–875.
Yu, C., Ji, S., Li, Q., 2016. Effects of porosity on seismic velocities, elastic moduli, and Poisson's ratios of solid materials and rocks. J. Rock Mech. Geotech. Eng. 8 (1), 35–49.
Zaouia, N., Elwartiti, M., Baghdad, B., 2005. Superficial alteration and soluble salts in the calcarenite weathering: case study of Almohade monuments in Rabat, Morocco. Environ. Geol. 48, 742–747.
Zerrouki, A.A., Géraud, Y., Diraisson, M., Baddari, K., 2019. A preliminary study of relationships between thermal conductivity and petrophysical parameters in Hamra Quartzites reservoir, Hassi Messaoud field (Algeria). J. Afr. Earth Sci. 151, 461–471.
Zerrouki, A.A., Géraud, Y., Dobbi, A., Diraisson, M., Baddari, K., Lebtahi, H., 2022. P-wave velocity anisotropy in Hamra Quartzites reservoir, Hassi Messaoud oil field in Algeria. Arabian J. Geosci. 15, 800.
Zhang, J., Shen, Y., Yang, G., Zhang, H., Wang, Y., Hou, X., Sun, Q., Li, 2021. Inconsistency of changes in uniaxial compressive strength and P-wave velocity of sandstone after temperature treatments. J. Rock Mech. Geotech. Eng. 13 (1), 143–153.

Abdelaali Rahmouni is currently an Assistant Professor of Physics at Faculty of Science Dhar El Mahraz, Sidi Mohamed Ben Abdellah University, Fez, Morocco. He obtained a BSc degree in Physics from Faculty of Science, Moulay Ismail University, Meknès, Morocco in 2005, a MSc degree in Physics of Condensed Matter from Faculty of Science, Chouaib Doukkali University, El Jadida, Morocco in 2008, and a PhD degree in Mechanics and Energy from Faculty of Science, Mohammed V University, Rabat, Morocco and University of Strasbourg, France in 2016. He has participated in accomplishing a number of national and international scientific research projects. His main research interests include rock mechanics, geotechnical engineering, energy phenomena of fluid transfer in rocks, conservation and restoration of historical heritage, characterization of construction materials, and seismic wave attenuation. He has published research papers in national and international journals in the field of mechanics, civil engineering and geophysics. He has presented lectures at conferences and other forums.